Development and testing of a synchronous-scanning underwater imaging system capable of rapid two-dimensional frame imaging

Thomas J. Kulp, Darrel Garvis, Randall Kennedy, Tom Salmon, and Keith Cooper

The design and construction of a synchronous-scanning underwater imaging system capable of rapid two-dimensional scanning are described. The imager employs a 7-W, all-lines, argon-ion laser in conjunction with a galvanometrically driven raster scanner and an image-dissector tube receiver. The imager is capable of directly generating real-time RS-170 video imagery. The results of an in-water test of the imaging system, in which a high-contrast imaging test pattern was imaged, demonstrate operating ranges of up to 4 attenuation lengths (AL) when the test was run at real-time frame rates, ranges of 5.1–5.5 AL when the system operated with an eight-frame running average, and ranges of 6.3 AL when a 128-frame running average was used. The system performance was compared with that of several floodlight/silicon-intensified-target TV camera configurations, which produced a maximum imaging range of ~2.6 AL. Also, an imaging configuration that used the raster-scanned beam of the laser as an illumination source for the silicon-intensified-target camera was tested. That system had an ultimate range of ~4 AL.

Introduction

The range at which objects can be imaged underwater is typically limited by the noise in the backscattered radiation generated in the water between the imaging system and its target.[1] The scatter is produced in the overlapping volume of the illumination source and the field of view (FOV) of the imaging device and is therefore called common-volume backscatter. In conventional underwater imaging systems that are composed of video cameras and wide-beam floodlights, the imaging range is limited when the variation in the common-volume backscatter exceeds the inherent contrasts of the target image. This is a result of the limited dynamic range of the camera. For a typical commercially available floodlight-illuminated imager, this limit occurs at a target distance of ~2 attenuation lengths (AL).

T. J. Kulp, D. Garvis, and R. Kennedy are with the Environmental Sciences Division, Lawrence Livermore National Laboratory, MS L-524, P.O. Box 5507, Livermore, California 94551-5507. T. Salmon and K. Cooper are with the Office of Salvage and Diving, Naval Sea Systems Command, Washington, D.C. 20362-5101.

Received 3 June 1992.
0003-6935/93/193520-11$06.00/0.

For the last two decades, novel experimental imaging systems based on the use of lasers have been devised to reduce the effects of common-volume backscatter and thus to increase the underwater visibility range.[1–14] These devices take advantage of either the unique spatial or temporal properties of laser radiation to discriminate against backscatter generated in seawater. The two primary techniques that are employed by these cameras are range gating[2–6] and synchronous scanning[6–12]; there have also been some novel variants of the latter.[13,14]

In range gating the target is illuminated with a short-duration laser pulse as it is imaged by a rapidly gated electronic camera. The camera gate is triggered to open following the round-trip time of flight of the laser pulse and remains open for a time equal to the laser-pulse duration. Scattered light received outside this temporal window is rejected.

In synchronous scanning the highly collimated nature of the laser beam is employed for spatial rejection of common-volume scatter. With this approach the laser is directed to illuminate the target at a single point, and scattered radiation from that point is collected in the well-collimated instantaneous field of view (IFOV) of a single-element detector. The overlap zone between these two volumes is then scanned in a line or raster fashion across the target to

produce a video image of the target. Because of the small overlap length of these two beams, the common volume is drastically reduced, and common-volume scatter is minimized. According to theoretical predictions, laser-based imaging systems should be capable of operation at ranges of up to 7 AL or more.[6,15]

In this paper we present the results of an effort to develop a synchronous, raster-scanning imager that is capable of real-time and near-time video frame rates. The underwater laser-imaging system (UWLIS) differs from earlier synchronous scanners in its ability to scan in two dimensions at conventional video frame rates (30 Hz). The performance of the UWLIS during an in-water tank test is described, where the imaging performance of the system was tested at target ranges of up to 6.3 AL (at a physical distance of 15.2 m). At ranges of <4 AL the imager was able to produce acceptable video images while operating at its full imaging bandwidth. At longer ranges, however, it was necessary to reduce the frame rate to improve the image signal-to-noise ratio. This was accomplished with a running frame averager. At ranges between 4 and 5 AL, an eight-frame average was used. Between 5.0 and 5.7 AL a 32-frame average was used (although an eight-frame average still produced usable imagery to 5.5 AL). To reach the ultimate range of 6.3 AL, a 128-frame average was used. The results of the test demonstrate that the imager was limited by the magnitude of the return signal and residual electronic noise and not by common-volume backscatter.

Relationship to Past Underwater Imaging Efforts

In developing and testing an underwater imaging system of this type, the factors that influenced the application of earlier systems should be considered. Although a great deal of effort has been devoted to the development of laser-based underwater imaging systems, there have been few operational implementations of them. This can, in general, be attributed to the practical limitations of the lasers that were used and their associated hardware. The commercially available green and blue-green sources that have appreciable transmission in seawater are the argon-ion (Ar^+) and the lamp-pumped, frequency-doubled Nd:YAG (2*Nd:YAG) lasers. Both operate with low electrical-to-optical conversion efficiencies and thus require a large amount of electrical power to be delivered to the underwater platform containing the imager. In past applications this was a serious restriction. Additionally earlier laser sources were not as reliable as current systems, especially when operating in a hostile environment such as on an undersea vehicle. This was also true of the mechanical scanning mechanisms required for rapid synchronous scanning and of the rapidly gated cameras needed for range-gated imaging. In the case of synchronous scanning, hardware limitations prevented operation at real-time video frame rates. Finally, although both types of laser-based approach were demonstrated to reduce the effects of scattered light, they were found to be photon or electrical noise limited at long ranges. Thus the systems were inherently restricted by the power of their laser source, their detector sensitivity, and the geometrical collection efficiency of their receiver optics. This was especially important for efforts whose goals were extremely long-range search or surveillance applications.

In recent years advances in technology have relaxed some of the hardware limitations. Although the existing commercially available laser sources continue to be the electrically inefficient Ar^+ and lamp-pumped 2*Nd:YAG, the ability to deliver electrical power over long underwater cables has improved. Thus it is increasingly possible to alocate the power required to operate a laser on moderately sized underwater platforms. Rapid increases in the development of diode-laser-based sources will further alleviate power-budget limitations. Diode-pumped 2*Nd:YAG sources operating at power levels of 3–5 W and efficiencies of a few percent or more should become available in the next few years. Assuming that 5 W of optical power are required, their use will reduce the electrical-power budget requirement for the laser from as high as 10 kW (for the Ar^+ laser) to ~ 500 W. General improvements in electro-optic technologies have also made laser and scanner hardware more reliable and adaptable to operation in rugged environments. In fact an Ar^+ laser-based underwater line scanner is now commercially available.[16]

Although these hardware improvements will improve the feasibility of implementing a reliable laser-based imager, issues of signal strength remain. Despite the fact that both laser-based approaches can drastically reduce backscatter, low return signals may still restrict operation to physical distances that are too low for some applications. Signal-strength issues are especially important when one is considering fast two-dimensional scanners, such as the UWLIS, which require high detector bandwidths (i.e., low pixel dwell times). Low signals inevitably lead to trade-offs among range, imaging bandwidth, and imaging field of view. Ultimately the utility of a laser-imaging system will be judged by the specific requirements of the application.

The UWLIS is intended specifically for use on remotely operated vehicles (ROV's) during deep-ocean salvage operations. Although very large imaging ranges (>300 m) are desired in this application, an extension of the visibility range to 60–80 m is sufficient to produce a significant saving in cost during salvage missions. Because of its two-dimensional imaging capability, the UWLIS is expected to fill a specific need in ROV operations that is not possible with other synchronous-scanning systems, such as line scanners. The real- and near-real-time frame rates of the UWLIS make possible operation in a stationary mode or in a mode in which platform speed is randomly varied. This is typical of the ROV operational environment, in which the platform is often maneuvered above and around rugged seafloor

terrains. Signal-to-noise (i.e., measuremental bandwidth) and resolution requirements do, however, limit the system to relatively narrow FOV's. In this respect the UWLIS can be considered a complementary device to line scanners, which permit larger swath scans but require forward vehicle motion and lower horizontal line rates.

UWLIS Imager Description

A diagram of a general synchronous-scanning imager is shown in Fig. 1. The device consists of a cw laser whose beam is scanned across the target area in some type of one- or two-dimensional scan pattern. In a line scanner a one-dimensional scan is used, and the motion of the platform provides the second dimension of the image. In a raster scanner the beam is scanned in two dimensions. The detector in the synchronous-scanning imager is typically a single-element device whose IFOV is collimated to a divergence that is slightly larger than that of the laser. The detector IFOV is directed to intersect the laser beam at the target and is scanned so that the intersection volume is maintained as the laser beam is swept. The signal-processing electronics amplify and format the detector signal so that it can be displayed as a two-dimensional target image.

The UWLIS is a synchronous-scanning imager of the raster-scanning type. Its optical layout is shown in Fig. 2. Earlier versions of the UWLIS have been tested and are described in other papers.[10–12] In general the ranges of the past designs were limited by scattering generated on the scanner optics. This motivated the construction of the current UWLIS, shown in Fig. 2, in which the laser transmission and signal return paths are completely separate. The laser-beam transmission optics consist of a pair of galvanometrically driven scan mirrors, whose concerted horizontal and vertical motions produce the raster scanning of the laser beam. The mirrors are

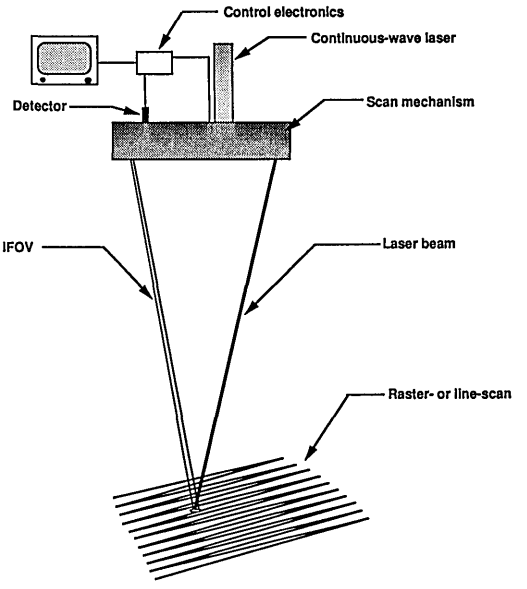

Fig. 1. General diagram of a synchronous-scanning imager.

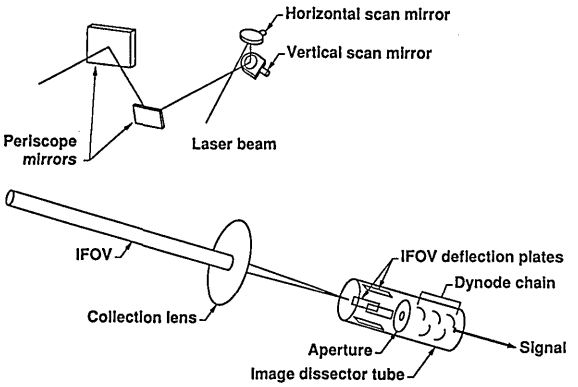

Fig. 2. Diagram of the optical layout of the UWLIS imager.

composed of beryllium substrates onto which are replicated aluminum reflective surfaces (with reflectivity of ~92% at the laser wavelengths). The horizontal mirror is scanned sinusoidally, with a frequency of 3933 Hz, while the vertical mirror is scanned by a sawtooth wave form with a sweep rate of 60 Hz. The beam from an all-lines (457–514-nm), argon-ion laser (Model 905, American Laser Inc., Salt Lake City, Utah) is injected into the scanner to intercept the horizontal-scan mirror. The laser power was nominally 5 W, but 7 W of power was being produced at the time of the test. From there it is reflected down to the vertical-scan mirror and out of the scanner to a periscope mirror assembly, from which it travels to the target. The maximum dimensions of the raster scan are 18° (horizontal) by 14° (vertical). The system FOV is currently limited by mechanical properties of the particular resonant horizontal scanner that is used. Technology does exist, however, for increasing that physical scan angle to 30°. Multiple-reflection scan configurations can also be used to achieve real-time optical scans of up to 60°.

The return signal from the target is detected and scanned with an image-dissector tube (Model R312, Hamamatsu Inc., Bridgewater, N.J.). Image-dissector tubes (IDT's) have been used in the past as receivers for other synchronously scanned imagers and for laser trackers.[6,7,17] They are essentially scanning photomultiplier tubes (PMT's), in which a signal generated at any small region of the photocathode can be selectively detected at the anode.

The operation of an IDT is illustrated in Fig. 3. In the photocathode region, photoelectrons to be interrogated are focused by a set of electrodes and deflected (by a set of x–y deflection plates) through a small aperture. The position of the interrogation region on the photocathode is determined by the voltages on

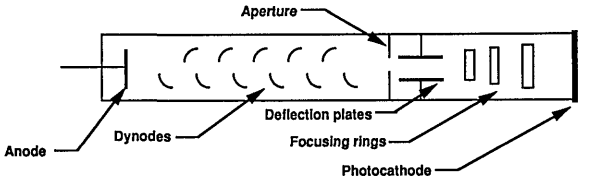

Fig. 3. Schematic of an IDT.

the deflection plates, while its size is determined by the size of the aperture and the magnification of the electron lens. After the photoelectrons pass through the aperture, they are multiplied by a dynode chain and collected at the anode, as in a normal PMT. The ability to position the interrogation region electronically on the photocathode makes it possible to scan this region electronically as well.

In the UWLIS, the IFOV of the IDT is raster scanned when the appropriate drive signals are applied to the deflection plates to scan the photocathode interrogation region. These drive signals are amplifications of signals from sensors monitoring the position of the scan mirrors. The IDT has a custom aperture size of 265 μm and an electronic lens magnification of 0.5, so the diameter of the photocathode collection area is 530 μm. The target region is imaged onto the face of the IDT with an $f/1.2$, 50-mm camera lens. These optics produce a circular IFOV with a divergence of 10.6 mrad—~10 times the divergence of the 1-mrad argon-ion laser beam. The oversized IFOV is necessary to permit synchronization at all positions in the raster because of the 2% scan distortion of the IDT. With this IFOV size, fully synchronized imagery can be produced over the full-system FOV.

The development of the UWLIS was accelerated by adapting an existing raster-scanning imager to accomplish the beam scanning and the generation of the RS-170 video signal. This imager is an IR flying-spot camera (Model 522, Inframetrics, North Billerica, Mass.). Mechanical raster scanning is used to generate video imagery in the IR, because inexpensive and reliable focal-plane array detectors operating in that wavelength range are not available. The only optical components used from the Inframetrics camera are the two galvanometers and their scan mirrors. Its signal-processing electronics and scan-mirror controllers are employed as the control electronics for the UWLIS.

To generate the raster scan, the horizontal galvo is driven at a rate of 3933 Hz by a sinusoidal drive signal. Each period of the sine wave generates two video lines. The horizontal galvo is a resonant device that runs freely. All other system timing is derived from its motion. The positions of both the horizontal and vertical mirrors are sensed continuously by a pair of optical sensors that measures the deflection of a light beam off the back of the mirrors. The signals from these sensors provide the feedback to lock the mirrors to their drive signals. The vertical galvo is an ordinary stepping-type scanner that is driven by a 60-Hz sawtooth wave to produce the vertical dimension of the raster scan. The imager generates fields every 1/60th s in which alternating lines are scanned and full frames every 1/30th s. To produce the correct line density for RS-170 video, each line is written out twice on the video screen, so that each horizontal line has one identical neighbor.

As we mentioned above, the horizontal galvo drive signal and the vertical galvo position sensor signal are amplified and used to drive the horizontal and vertical deflection plates of the IDT. Each signal is amplified to ±240 V by a high-voltage operational amplifier. The horizontal drive requires a phase-delay control to compensate for delays in the electronics. (The sine wave used to drive the IDT horizontal scan is actually the wave from the previous galvo scan that has been delayed by one full cycle.)

In addition to the drive signals the R312 IDT requires a voltage drop of 300 V across its focusing electrodes and a variable voltage drop of up to 1200 V across its dynode chain. The signal collected at the anode is amplified by a standard PMT preamplifier (Model C1053, Hamamatsu) and matched to span the voltage range required at the input of the Inframetrics scanner. In the Inframetrics processing electronics the preamp output is directed through a gain adjustment stage and then digitized by an 8-bit analog-to-digital converter. The scan conversion to the RS-170 video is then accomplished by a digital-to-analog circuit that stores the video lines in a RAM buffer and reads them out at the appropriate line rate (with each line being read out twice to adjust for the mismatch between the frame rates of the two formats). As part of the readout process the camera also accomplishes a linearization of the horizontal scan, which is required to correct for the sinusoidal variation of scan angle with time. Scan linearization is accomplished by using varying delays (controlled by values saved in a lookup table) between the points at which successive pixels are read out of the RAM buffers. During the testing of the system a digital frame averager (Model DS-50, Quantex, Rockville, Md.) was inserted between the video output of the system and the video display and recorder. This device allowed real-time running frame averages (between 2 and 128 frames in multiples of two) to be made and displayed.

A diagram of the test configuration of the UWLIS imaging head is shown in Fig. 4. The IDT is attached to a mount that allows it to be tilted to adjust the intersection plane of the IFOV and laser as the target range is changed. During the tests only the

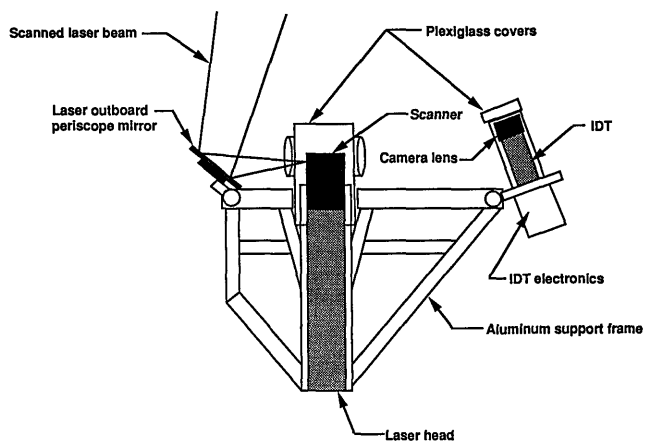

Fig. 4. Diagram of the test configuration of the UWLIS imaging head.

front portion of the scanner was immersed beneath the surface of the water. This was accomplished by mounting the imager head framework in a near-vertical orientation, so that its front portion was under the water surface. Figure 5 contains a photograph of the UWLIS imaging head during testing. The scanner assembly and the IDT were enclosed in Plexiglas covers (shown in Fig. 4) that allowed these components to be submerged. Each cover contains a flat AR-coated silica window to transmit the light to and from the target. The outboard laser periscope mirror was located outside the Plexiglas cover and was thus directly immersed in the water. As the position of the target changed, the tilt of the outboard laser mirror and the IDT were adjusted to maintain intersection at the target. Additionally the tilt of the whole UWLIS framework could be adjusted.

UWLIS Range Estimation

Detailed calculations of the maximum-range performance of synchronously scanned imaging systems have been provided in the past,[1,8] where the effects of both single and multiple scattering and the total photon return signal were considered. In the test conditions described in this paper, it was found that the ultimate range of the UWLIS was determined primarily by the strength of the return signal and not by common-volume backscatter. Because laser power and optical collection limitations may in general impose a greater restriction on the range of the scanner than common-volume backscatter, it is useful to estimate the signal-limited range of the system. This can be done by use of a simple calculation and the existing data.

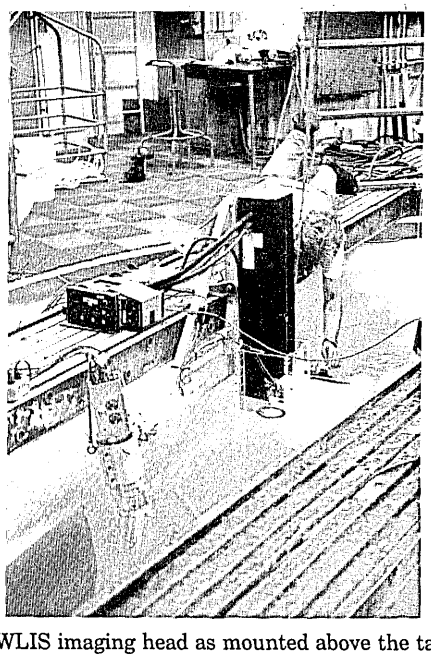

Fig. 5. UWLIS imaging head as mounted above the tank during testing. The only components immersed in the water were the IDT (on the left side of the frame) and the scanner (below the laser head, in the center of the frame). Each is enclosed in a Plexiglas protecting housing.

The power of the return signal of the UWLIS is given by

$$P_T(R) = \sum_i P_{li}\eta_{TL}(\lambda_i)\tau^2(R, \lambda_i)\beta(\lambda_i)\eta_{RL}(\lambda_i)\Omega(R), \quad (1)$$

where the sum is made over all the lines of the argon-ion laser and

P_{li} is the power of the ith laser line,
$\eta_{TL}(\lambda_i)$ is the optical transfer efficiency of the transmitter optics,
$\tau(R, \lambda_i)$ is the seawater transmittance at the range R and the laser wavelength,
$\beta(\lambda_i)$ is the target reflectance,
$\eta_{RL}(\lambda_i)$ is the optical transfer efficiency of the receiver optics,
$\Omega(R)$ is the solid angle of collection of the return optics.

The solid angle of collection of the return is given by

$$\Omega(R) = A_0/R^2, \quad (2)$$

where A_0 is the area of the receiver collection aperture.

Assuming (for the purpose of this estimate) no contribution from water backscatter, the noise of the system results from the electrical noise of the preamplifier, the dark-current noise of the IDT, and the shot noise in the return signal. The overall signal-to-noise ratio (S/N) is improved by frame averaging in proportion to $N^{1/2}$ (where N is the number of averaged frames). The S/N of the return signal can be obtained by dividing the signal expression in Eq. (1) by the detection system noise equivalent power (equal to $P_n N^{-1/2}$):

$$\mathrm{S/N}(R) = [KP_l\tau^2(R)A_0R^{-2}]/P_nN^{-1/2}, \quad (3)$$

where K contains all remaining terms, and the sum over laser lines has been replaced by a wavelength-averaged laser power and an average water attenuation coefficient.

Equation (3) and the results of the tank test can be used to extrapolate the imager performance to other ranges, water conditions, and degrees of frame averaging (i.e., under different R, N, or τ). Assuming that an acceptable S/N was achieved in certain conditions at the test, Eq. (3) can be used to determine the laser power required to achieve the same S/N in different conditions. This is done by dividing the expression for the observed S/N by the expression for the S/N at the expected conditions, setting the result equal to one, and solving for the expected laser power:

$$P_l = P_{l,\mathrm{obs}}\{(R/R_{\mathrm{obs}})^2(N_{\mathrm{obs}}/N)^{1/2}[\tau^2_{\mathrm{obs}}(R)/\tau^2(R)]\}, \quad (4)$$

where the subscript indicates the conditions in which the observed signal was acquired. Note that this assumes that one is imaging a target of the same reflectivity and contrast as that used in the tests, which is quite high. Often, for real-world targets of

interest, contrast and reflectivity will be lower. According to Eq. (3), the S/N in given conditions will scale linearly with the target reflectivity. In addition the imager range performance will scale according to Eq. (4). In this paper we focus on the extrapolation of the results obtained when the test target was used. However, given a specified target reflectivity, the above equations and our results can be used to predict range.

Tank-Test Description

The in-water tank tests of the UWLIS prototypes were carried out on three occasions in free-ascent dive towers located at two different Navy facilities (the Naval Amphibious Base at Coronado, Calif. and the Navy Salvage and Diving Training Facility at Panama City, Fla.). Unless otherwise noted the results presented in this paper were obtained at the last tank test, which occurred at the Florida facility.

A free-ascent dive tower is a large, cylindrical, above-ground water tank used for training divers to surface from pressurized submersible vessels. The dimensions of the towers located at the two test locations are virtually identical. A diagram of the tank is in Fig. 6. It has a diameter of 6 m and a depth of 15.2 m and is capable of holding 390,180 L of water. During the tests the optical properties of the water column were altered to simulate different seawater conditions. This was accomplished by adding controlled amounts of Maalox (to increase the water-scattering coefficient) and nigrosin dye (to increase the water-absorption coefficient). During a tank test the additions and the imaging trials were carried out over a period of several days. To maintain stable water conditions during this time, it was necessary to disconnect the tank filters from the recirculation loop. The circulation pumps were left operating, however, so that the water would be continually stirred and the Maalox particles would remain in solution.

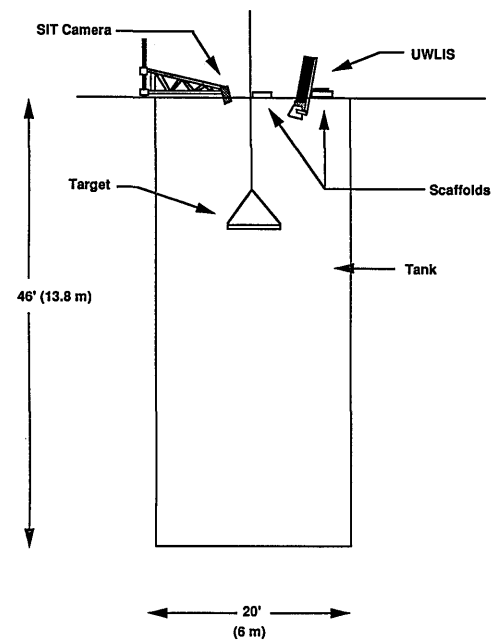

Fig. 6. Diagram of the free-ascent diving tower. The 13.8-m depth is the depth at the edge; the center depth is 15.2 m.

During the second and third tests, several other imaging configurations were tested in parallel with the UWLIS (see Table 1). Most of them consist of a conventional underwater silicon intensified target (SIT) camera (Osprey Electronics, Dyce, Aberdeen, Scotland, Model OE-1323) that was illuminated by various types or orientation of floodlights. They were used primarily to replicate the imaging conditions that are currently employed on Navy ROV's [System 2 (S2)] and to provide a comparison to the UWLIS. In some cases attempts were made to improve the performance of the conventional imaging arrangement. System 3 (S3) used a blue-transmitting filter to reject backscattered radiation at nonblue wavelengths; this light contributes relatively little to the total target return signal. System 4 (S4) is intended to improve imaging performance by widening the separation between the illumination source and the camera. System 5 (S5) used a thallium–iodide lamp that emits over a narrow bandwidth (at 535 nm) in the blue-green spectral range. The final floodlight-illuminated camera, System 6 (S6), was intended to improve performance by narrowing the beamwidth of the floodlights, thus reducing the near-field common volume.

Two SIT camera systems were tested that used the laser as their illumination source. System 7 (S7) utilized the laser raster scan to illuminate the FOV of the SIT camera. As will be seen, the distinct illumination pattern of the laser scan allowed that configuration to achieve significantly improved ranges over the floodlight-based systems. Similar results were found with System 8 (S8), in which the laser beam was spread with a set of diverging optics to illuminate the target with a narrow cone of radiation.

The target that was imaged during the tests con-

Table 1. Imaging Configurations Used at Tests II and III

System	Description
S1	UWLIS with 54-in. (137.16-cm) IDT–mirror separation
S2	Tungsten–halogen floodlight (wide-beam)-illuminated SIT camera, 25-in. (63.5-cm) separation[a]
S3	S2 with blue transmission filter (4-96, Corning Glass Company, Corning, N.Y.) mounted on the camera lens
S4	S2 with 8-ft. (2.4-m) lamp–camera separation
S5	Thallium–iodide, floodlight-illuminated[b] SIT camera, 63.5-cm lamp–camera separation
S6	S2 using narrow-beam tungsten–halogen floodlight[c]
S7	Raster-scanned, laser-illuminated SIT camera, 43-in. lamp–camera separation
S8	Flood laser-illuminated SIT camera, 63.5-cm laser–camera separation

[a]Two 150-W halogen floodlights, Deep-Sea Power and Light (San Diego, Calif.) Model SL-24/150, specular reflectors Model NF-1.

[b]One 450-W thallium–iodide floodlight with diffuse reflector on loan from Deep-Sea Power and Light.

[c]One 250-W halogen spot floodlight, Deep-Sea Power and Light Model MXD-SP.

sisted of a square (112 cm × 112 cm) steel-screen panel that was suspended in the water by a rope block and tackle assembly. A standard Air Force imaging target (Applied Image, Rochester, N.Y.) with dimensions slightly less than that of the frame was cemented to a Lucite sheet and placed on the panel. To avoid chlorine bleaching in the tank, the target was sprayed with a clear lacquer before being placed in the water.

Water Additions

The imaging tests were performed in clear water and in 10 levels of optically degraded water. At each successive addition of Maalox or nigrosin dye the extinction coefficient of the water was measured with a 10-cm-path-length transmissiometer (Sea Tech, Inc., Corvallis, Ore.) that used a light source peaked at 660 nm. During the second tank test an attempt was made to make these measurements with a blue-green transmissiometer (Moniteq, Inc., Concord, Ont., Canada) that used a light-emitting-diode source peaked at 530 nm. That device would not, however, produce reliable measurements at the time of the test.

Because the Sea Tech transmissiometer measured transmittance in the red, it was necessary to extrapolate the measured water clarity (at 660 nm) to the relevant blue-green wavelength (500 nm, which is approximately halfway between the two dominant laser lines of the argon-ion laser at 488 and 514 nm) according to the spectral absorption and scattering characteristics of the dye and the Maalox. These spectral characteristics were obtained from a series of measurements conducted at the Scripps Institute of Oceanography Visibility Laboratory.[18] The spectral variation in the increase in the absorption coefficient (Δa) for an increase in the nigrosin dye concentration of 270 μg/L is given in Table 2. Unfortunately these measurements were not made to wavelengths as great as 660 nm, so that the value in Table 2 is an extrapolated one. The absorption properties of the nigrosin/water mixture at 500 nm were estimated according to

$$a(500\ \text{nm}) = 1.32\, a(660\ \text{nm}). \tag{5}$$

The scattering properties of the water were calculated according to

$$\Delta s(\lambda)/\Delta s(536\ \text{nm}) = [536/\lambda]^{1.44}, \tag{6}$$

where Δs is the increase in the scattering coefficient in units of inverse meters. The data obtained at the Scripps Institute of Oceanography Visibility Laboratory show that

$$\Delta s(536\ \text{nm}) = 1\ \text{m}^{-1} \tag{7}$$

for a volumetric increase in Maalox concentration of 20 parts in 10^6.

Results and Discussion

Water Conditions

During the additions to the tank it was found that the chlorine present in the water bleached the nigrosin over time. Thus nigrosin was added only for the first three water-clarity levels. For those levels it was necessary to make dye and Maalox additions to the tank separately, because the transmissiometer is incapable of measuring the individual contributions of a and s to α. For example, if a quantity of Maalox is added to the tank, the measured change $\Delta\alpha(660)$ can be considered to be entirely a result of a change in s, and Eq. (6) can be used to calculate the corresponding Δs at 500 nm. This number may then be added to the $\alpha(500)$ value before the addition to obtain the current $\alpha(500)$. Clear water $\alpha(500)$ and $\alpha(660)$ were assumed to be 0.090 and 0.400 m^{-1}, respectively, according to the data of Smith and Baker.[19]

The optical properties of the 10 levels of water degradation at which images were collected are listed in Table 3. Included there are the measured values of $\alpha(660)$, the values of $a(660)$, $s(660)$, $a(500)$, and $s(500)$ that were calculated from the transmissiometer readings, and the values of a, s, and α at the two wavelengths that were predicted on the basis of the amount of dye and Maalox added. Finally the magnitude of an AL for each level is given.

Note that the table shows some disagreement among the predicted values and those inferred from the measurements, i.e., the latter fall slightly short of the former. In addition to the dye bleaching, we observed that the Maalox particles appeared to be plating out on the walls of the tank over time. This problem was minimized by frequently stirring the tank with air released from outlets along the tank walls. Depth-profile measurements taken with the transmissiometer at various positions in the tank confirmed that the water was uniformly mixed and that stratification of the Maalox was not so severe as in the previous test.[12]

Images

Images collected during the test were recorded on VHS videotape. Still photographs that were made from the tape are presented in this section. It should be noted that some loss in image quality

Table 2. Spectral Absorption Properties of Nigrosin Dye[a]

Wavelength (nm)	450	491	536	567	585.5	614.5	631	660
Δa (m^{-1})	0.78	0.95	1.08	1.12	1.10	1.00	0.82	0.75[b]

[a] Δa for 270 μg/L.
[b] Extrapolated value.

Table 3. Predicted and Measured Water Conditions[a]

Degradation Level	Measured $a(660)$	Predicted Values					
		$s(660)$	$\alpha(660)$	$a(500)$	$s(500)$	$\alpha(500)$	AL(500)
Clear	0.400	0.0260	0.426	0.0257	0.0388	0.0645	0.98
1	0.405	0.0560	0.461	0.0321	0.0839	0.116	1.8
2	0.414	0.0803	0.494	0.0443	0.120	0.164	2.5
3	0.424	0.0803	0.504	0.0573	0.120	0.177	2.7
4	0.424	0.127	0.551	0.0573	0.190	0.248	3.8
5	0.424	0.163	0.587	0.0573	0.243	0.301	4.6
6	0.424	0.187	0.611	0.0573	0.278	0.336	5.1
7	0.424	0.217	0.641	0.0573	0.323	0.381	5.8
8	0.424	0.241	0.665	0.0573	0.359	0.416	6.3
9	0.424	0.269	0.693	0.0573	0.400	0.458	6.9
10	0.424	0.297	0.721	0.0573	0.441	0.499	7.6
		Inferred from Measurement					
		$s(660)$	$\alpha(660)$	$a(500)$	$s(500)$	$\alpha(500)$	AL(500)
Clear	0.400	0.0260	0.426	0.0260	0.0388	0.0648	0.99
1	0.405	0.0560	0.461	0.0324	0.0839	0.116	1.8
2	0.405	0.0817	0.487	0.0324	0.122	0.154	2.3
3	0.416	0.0817	0.498	0.0473	0.122	0.169	2.6
4	0.416	0.113	0.529	0.0473	0.168	0.215	3.2
5	0.416	0.147	0.563	0.0473	0.218	0.265	4.0
6	0.416	0.165	0.581	0.0473	0.244	0.291	4.5
7	0.416	0.192	0.608	0.0473	0.285	0.332	5.1
8	0.416	0.200	0.616	0.0473	0.296	0.344	5.2
9	0.416	0.225	0.641	0.0473	0.333	0.380	5.8
10	0.416	0.244	0.660	0.0473	0.361	0.409	6.3

[a]All a, s, and α are in units of inverse meters. The column labeled AL indicates the number of attenuation lengths (at 500 nm) to the bottom [50-ft (15.2-m) depth].

occurs during this transfer. In addition it should be noted that imaging performance is discussed only qualitatively here. No effort has yet been made to compare these images quantitatively (i.e., by using contrast S/N and modulation transfer function analysis).

Floodlight-Illuminated SIT Camera

The tungsten–halogen floodlight-illuminated SIT camera configuration (S2 in Table 1), currently used on ROV missions, was strongly affected by common-volume backscatter at ranges between 1 and 2 AL and was completely limited by backscatter beyond 2 AL. Attempts to improve range by using the spectrally filtered camera (S3), the wider camera–lamp separation (S4), and the blue-green emitting thallium–iodide lamp (S5) produced no significant differences. The use of the narrow-beam floodlight (S6) extended the camera range from 2.0 to 2.6 AL. No attempt was made to image with the narrow-beam floodlights at lamp–camera separations larger than 25 in. (63.5 cm), although it is likely that this would have further increased the range. Figure 7 contains images of the target produced at ranges of 0.99, 1.8, and 2.6 AL by the SIT/narrow-floodlight combination, which was the best floodlight-based system tested.

(a) (b) (c)

Fig. 7. Images produced by the narrow-beam, floodlight-illuminated SIT camera (S6). The conditions in which the images were made are (a) 0.99 AL (clear water), (b) 1.8 AL (level 1), and (c) 2.6 AL (level 3). The target distance was 15.2 m in each case.

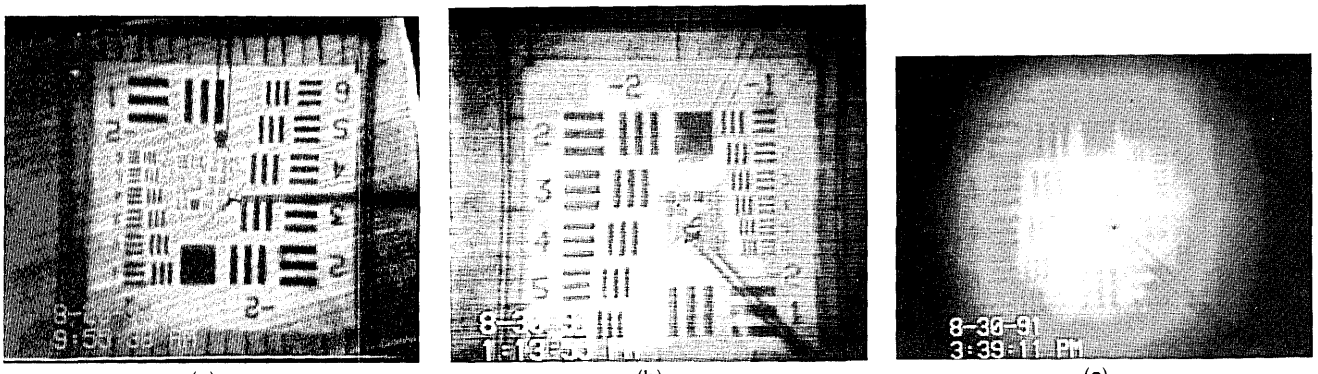

(a) (b) (c)

Fig. 8. Images produced by the raster-scanned, laser-illuminated SIT camera (S7). The conditions in which the images were made are: (a) 0.99 AL (clear water), (b) 2.6 AL (level 3), and (c) 4.0 AL (level 5). The target distance was 15.2 m in each case.

Laser-Illuminated SIT Camera

As in earlier tank tests[10,12] the raster-scanned, laser-illuminated SIT camera performed significantly better than the floodlight-illuminated configurations. Images obtained with it are shown in Fig. 8 at ranges of 0.99, 2.6, and 4.0 AL. The system had no trouble imaging at all degradations through level 4 water (0.99–3.2 AL). Imaging was still possible at 4.0 AL (level 5); however, the backscatter limit was judged to occur beyond that point. The results with the flood-laser-illuminated SIT camera were similar to those of the raster-scanned laser. In that system the diverging laser beam had nearly the same dimensions as the raster-scanned laser. The diverging laser does, however, form a Gaussian intensity profile on the target, while the scanned laser creates a more uniform illumination. In both laser-illuminated SIT configurations the improvement over the floodlight illumination can be attributed to the well-defined beam shape produced by the laser.

UWLIS

The performance of the UWLIS was superior to that of any of the SIT configurations, with an ultimate range of ~6.3 AL. Imaging was attempted with the UWLIS at all 10 levels of water degradation. Images obtained at ranges of 1.8, 2.3, 3.2, 5.1, 5.8, and 6.3 AL are shown in Fig. 9. At ranges up to 4 AL, only

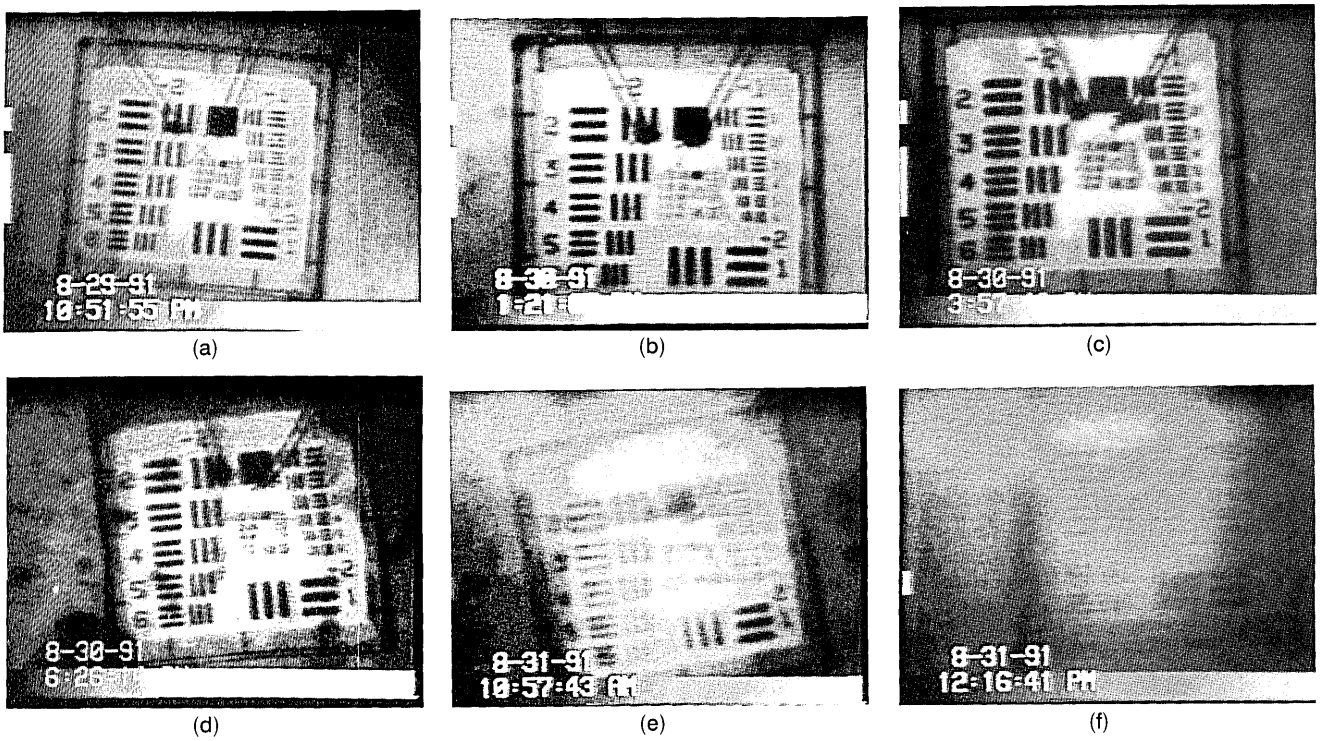

(a) (b) (c)

(d) (e) (f)

Fig. 9. Images produced by the UWLIS (S1). The conditions in which the images were made are (a) 1.8 AL (level 1), real-time frame rates; (b) 2.6 AL (level 3), real-time frame rate; (c) 4.0 AL (level 5), eight-frame running average; (d) 5.1 AL (level 7), eight-frame running average; (e) 5.8 AL (level 9), 128-frame running average; (f) 6.3 AL (level 10), 128-frame running average. The target distance was 15.2 m in each case.

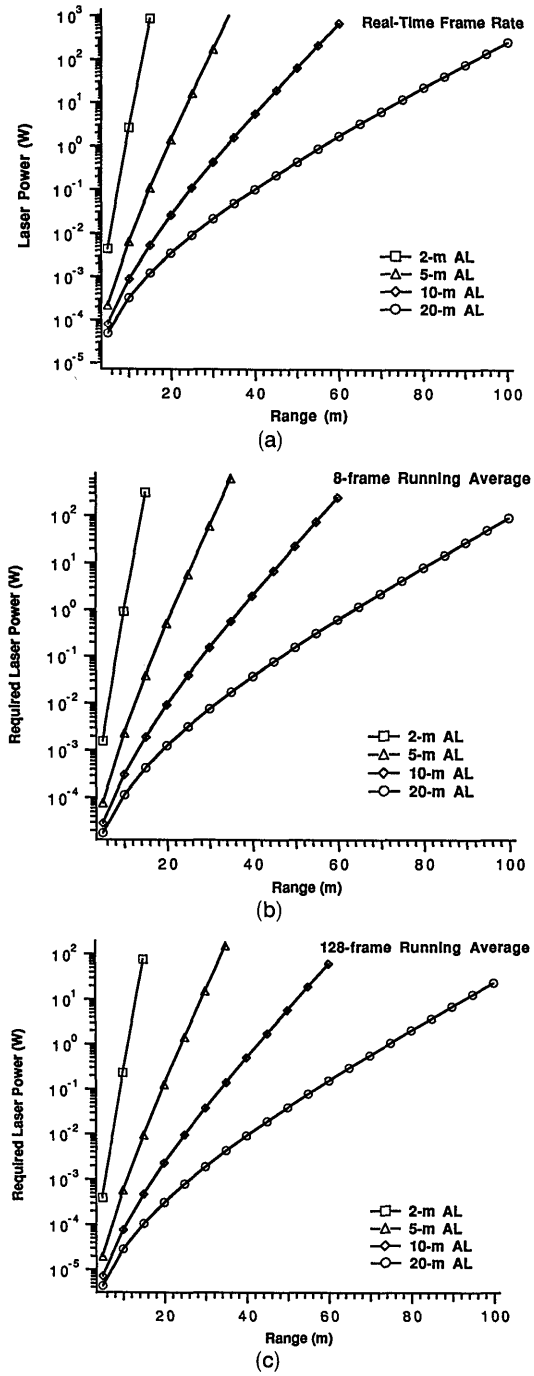

Fig. 10. Projected laser power required to image as a function of range in four different grades of seawater, ranging from AL of 2–20 m. The three graphs correspond to (a) real-time imaging rates, (b) eight-frame running averaging, and (c) 128-frame running averaging.

real-time imaging (30-Hz frame rate) was used in recording and displaying the images. Beyond this point, running frame averaging was used to reduce image noise. The number of frames averaged was selected to reduce the noise to the point that it was not visually noticeable. This again was a subjective judgment. Between 4 and 5 AL a running frame average of 8 frames was used. Between 5 and 5.7 AL, a 32-frame running average was used to reduce shot noise. It should be noted, however, that an 8-frame running average produced usable (although noisier) images at ranges up to 5.5 AL. This is important, since there may often be a trade-off between image noise and the amount of platform motion that is tolerable. Finally, at ranges between 5.8 and 6.3 AL, a 128-frame running average was selected to produce a visually clear image.

Although particulate scattering did not have a significant impact on the system range, there was an apparent loss in image contrast at the lowest water clarities (e.g., the images obtained at levels 9 and 10), which results from the spread in the laser beam caused by forward scattering and by backscatter. Because the IFOV has a divergence that is 10 times that of the laser, the system resolution is determined primarily by the laser spot size. In typical ocean waters, where the narrow-angle forward scattering is stronger than with the Maalox/Nigrosin mix, it is possible that the spatial-frequency degradation will be greater than that observed in the test.

Range Extrapolations

By using the results of the tank tests and Eq. (4), the performance of the UWLIS can be extrapolated to longer physical distances. The results of these extrapolations are shown in Fig. 10. Each graph indicates the laser power required for imaging to be permitted as a function of a physical target range under four different water qualities. The graphs differ in the number of averaged frames that are assumed. In all cases the calculations indicate the laser power required for a S/N to be produced that is equal to that measured in level 10 water at a 128-frame running average. Thus, if real-time frame rates are assumed (i.e., no averaging), a similar S/N can be expected at a physical range of 52 m in 15-m AL water, when a 7-W laser is used. Similarly ranges of 60 and 70 m are predicted when a 8- or 128-frame running average in 15-m water if 7 W of laser power are used.

Conclusion

The test results indicate that the UWLIS is capable of extending the underwater imaging range beyond that attained by several variations of the conventional floodlight-illuminated SIT camera system. The ultimate range achieved for this type of system is determined by the laser power, optical collection geometry, and the degree of frame averaging that is used. Specific observations concerning the implementation of this system are summarized as follows:

(1) As with other imagers based on cw lasers, the UWLIS will require a large amount of power (10 kW) to operate. This will be reduced as the development of high-power, blue-green, diode-pumped lasers occurs.

(2) The high scan rates of the UWLIS permit real-time video imaging to ranges of ~4 AL. The frame averaging used beyond that point will limit the

amount of platform motion that can be tolerated while clear images are being made. Preliminary tests were carried out at the tank test in which moving objects were imaged. They indicated that image motion such as that which might be expected on a slowly moving ROV can be tolerated at up to an eight-frame running average, which permits usable imaging at ranges up to 5.5 AL. At higher levels of averaging, it will be necessary that the platform remain stationary.

(3) Mechanical limitations of the horizontal scanner limit the present imager to a horizontal FOV of 18°. Improved resonant scanners permitting mechanical sweeps of up to 30° are now available. In addition, multiple-reflection scan configurations may permit optical scans of up to 60° to be achieved at the present scan rates.

(4) The two-dimensional scanning UWLIS is suitable for operations in which the platform is to remain stationary or is to move in a random fashion. This may be contrasted with a line scanner, which is suited to wide-swath searches from a towed platform. Ultimately it seems logical to produce an imager that is capable of both modes of operation since they share many of the same optomechanical components.

This research was performed under the auspices of the U.S. Department of Energy by Lawrence Livermore National Laboratory under contract W-7405-ENG-48.

References

1. C. J. Funk, S. B. Bryant, and P. J. Heckman, Jr., *Handbook of Underwater Imaging System Design,* NUC-TP-303. (Ocean Technology Department, Naval Undersea Center, San Diego, Calif., 1972).
2. T. Keil, A. Immarco, and M. Kerpchar, "Recent underwater range-gated measurements," in *Underwater Photo-Optical Instrumentation Applications II,* C. N. DeMund, ed., Proc. Soc. Photo-Opt. Instrum. Eng. **12,** 1–11 (1968).
3. P. Heckman, Jr., and R. T. Hodgson, "Underwater optical range gating," IEEE J. Quantum Electron. **QE-3,** 445–448 (1967).
4. L. H. Gilligan, "Range-gated underwater viewing," in *Underwater Imaging,* D. J. Holloway, ed., Proc. Soc. Photo-Opt. Instrum. Eng. **980,** 36–41 (1988).
5. N. H. Witherspoon and J. H. Holloway, "Feasibility testing of a range-gated laser-illuminated underwater imaging system," in *Ocean Optics X,* R. W. Spinrad, ed., Proc. Soc. Photo-Opt. Instrum. Eng. **1302,** 414–420 (1990).
6. L. E. Mertens, "New techniques," in *In-Water Photography, Theory and Practice* (Wiley–Interscience, New York, 1970), pp. 323–359.
7. F. S. Replogle and W. J. Stachnik, "Factory acceptance and extended tests of LOOK SEA underwater viewing system," Rep. TR4929 (U.S. Navy, Naval Underwater Systems Center, New London Laboratory, New London, Conn., 1975).
8. H. Hodara and W. H. Wells, "Synchronous scanning," presented at the AGARD Conference No. 77 on Electromagnetics of the Sea, Nevilly-sur-Seine, France, 1970.
9. B. W. Coles, "Recent developments in underwater laser scanning systems," in *Underwater Imaging,* D. J. Halloway, ed., Proc. Soc. Photo-Opt. Instrum. Eng. **980,** 42–52 (1988).
10. T. G. McRae, T. J. Kulp, D. Garvis, R. Kennedy, and T. Salmon, "Design and preliminary evaluation of an underwater laser-based imaging system," in *Ocean Optics IX,* M. A. Blizard, ed., Proc. Soc. Photo-Opt. Instrum. Eng. **925,** 351–362 (1988).
11. T. J. Kulp, D. Garvis, R. Kennedy, and T. G. McRae, "Current status of the NAVSEA synchronous scanning laser-imaging system," in *Underwater Imaging,* D. J. Halloway, ed., Proc. Soc. Photo-Opt. Instrum. Eng. **980,** 57–65 (1988).
12. T. J. Kulp, D. Garvis, R. Kennedy, and T. Salmon, "Results of the second tank trial of the LLNL/NAVSEA underwater laser imaging system," in *Ocean Optics X,* R. W. Spinrad, ed., Proc. Soc. Photo-Opt. Instrum. Eng. **1302,** 398–413 (1990).
13. S. Q. Duntley, R. W. Austin, R. L. Ensminger, T. J. Petzold, and R. C. Smith, "Experimental TVI system report: Part I, July 1974; Part II, October 1974," Tech. Rep. 74-1 (Scripps Visibility Laboratory, Scripps Institute of Oceanography, University of California, San Diego, La Jolla. Calif., 1974).
14. P. J. Heckman and P. D. McCardell, "A real-time optical mapping system," in *Ocean Optics V,* R. E. Stevenson and M. B. White, eds., Proc. Soc. Photo-Opt. Instrum. Eng. **160,** 189–196 (1978).
15. L. E. Mertens and F. S. Replogle, Jr., "Use of point spread and beam functions for analysis of imaging systems in water," J. Opt. Soc. Am. **67,** 1105–1117 (1977).
16. Available from Spectrum Engineering Inc., San Diego, Calif.
17. B. D. Fitzgerald, "Development of the automatic laser tracker," J. Soc. Motion Pict. Telev. Eng. **78,** 26–28 (1969).
18. T. J. Petzold, "Volume scattering functions for selected ocean waters," Tech. Rep. 72-78 (Scripps Visibility Laboratory, Scripps Institute of Oceanography, University of California, San Diego, La Jolla, Calif., 1972).
19. R. C. Smith and K. S. Barker, "Optical properties of the clearest natural waters (300–800 nm)," Appl. Opt. **20,** 177–184 (1981).